Nuclear Materials and Energy 11 (2017) 20–24

Contents lists available at ScienceDirect

Nuclear Materials and Energy

journal homepage: www.elsevier.com/locate/nme

Erosion at the inner wall of JET during the discharge campaign 2013–2014

S. Krat[a,b,*], M. Mayer[b], I. Bykov[c], C.P. Lungu[d], G. de Saint Aubin[b], A. Widdowson[e], I.S. Carvalho[f], JET contributors[g,1]

[a] National Research Nuclear University "MEPhI", Moscow Kashirskoe shosse 31, 115409, Russia
[b] Max-Planck-Institut für Plasmaphysik, Boltzmannstr. 2, 85748 Garching, Germany
[c] Fusion Plasma Physics, Royal Institute of Technology (KTH), Teknikringen 31, Stockholm 10044, Sweden
[d] NILPRP, Bucharest, Str. Atomistilor, Nr. 409, Romania
[e] CCFE, Culham Science Centre, Abingdon, Oxfordshire OX14 3DB, UK
[f] Instituto de Plasmas e Fusão Nuclear, Instituto Superior Técnico, Universidade de Lisboa, P-1049- 001, Lisboa, Portugal
[g] EUROfusion Consortium, JET, Culham Science Centre, Abingdon, OX14 3DB, UK

ARTICLE INFO

Article history:
Received 27 October 2016
Revised 28 January 2017
Accepted 15 February 2017
Available online 29 March 2017

ABSTRACT

The erosion of Be and W marker layers was investigated using long-term samples containing marker layers during the second ITER-like wall discharge campaign 2013–2014 (ILW-2). The samples were mounted in Be coated Inconel tiles between the inner wall guard limiters (IWGL). They were analyzed using elastic backscattering (EBS) before and after exposure. All samples showed noticeable erosion. The results were compared to the data for Be and W erosion rates for the first 2011–2012 JET ITER-like wall (ILW-1) campaign, and to the data for C erosion during the 2005–2009 campaign when JET was operated with a carbon wall. The mean W erosion rates and the toroidal and poloidal distributions of the W erosion were nearly the same for the ILW-1 and ILW-2 campaigns. The mean erosion rate of Be during the ILW-2 campaign was smaller by a factor of about two compared to the ILW-1 campaign.

1. Introduction

Erosion and redeposition of plasma facing materials are important processes that influence component lifetime and hydrogen isotope inventory in nuclear fusion devices. During the carbon-dominated operational phases of JET thick redeposited layers were observed in many areas of the device [1–4]. These layers contained large amounts of deuterium due to codeposition [5,6].

Before the start of the experimental campaign 2011–2012 [7], the wall and the divertor of JET were changed and the ITER-like wall (JET-ILW) with W and Be plasma-facing surfaces was installed [8]. The JET-ILW uses bulk beryllium on Inconel carriers for the inner wall guard limiters (IWGL) and outer wall limiters. In areas of increased heat flux W-coated carbon fibre composite (CFC) tiles are used for some IWGLs with recessed centre sections. Between the IWGLs Be coated Inconel tiles are installed. Tungsten coated CFC tiles are used in the divertor with a single belt of bulk tungsten tiles in the center part of the divertor.

The JET-ILW was shown to affect the erosion-deposition patterns [9–12] and fuel retention [13] as compared to the previous full carbon device. This includes a substantial decrease of erosion from the recessed areas of the inner wall (RAIW) between the IWGLs [11], which was identified as an important net source of carbon and beryllium redeposited in the divertor [14–17]. This decreased erosion was accompanied by a decrease of the impurity content of the plasma [18] and decreased deposition of material on divertor tiles [10] and in remote areas of the divertor [12].

However, during the 2011–2012 (ILW-1) campaign the initial discharge power was relatively low and was continuously increased until it reached the highest power loads only near the end of the campaign [19]. The total input energy for ILW-1 was 150.6 GJ, with a campaign averaged input power of 2.35 MW. Most plasmas had the inner strike point on the vertical inner divertor surface (Tile 3) and the outer strike point on the central bulk tungsten surface (Tile 5) [10]. It is therefore of crucial importance to confirm the positive results of decreased erosion/deposition and fuel retention, as obtained during the ILW-1 campaign, also for

* Corresponding author.
E-mail addresses: stepan.krat@gmail.com, sakrat@mephi.ru (S. Krat).

[1] See the Appendix of F. Romanelli et al., Proceedings of the 25th IAEA Fusion Energy Conference 2014, Saint Petersburg, Russia

http://dx.doi.org/10.1016/j.nme.2017.02.026

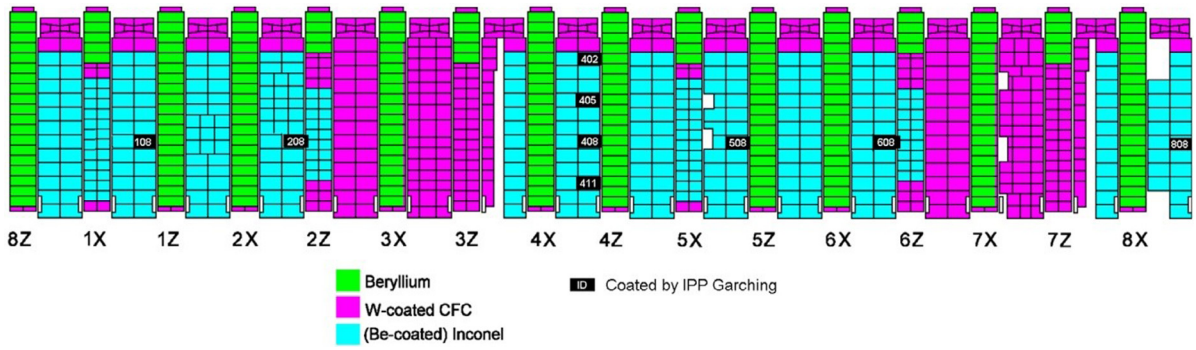

Fig. 1. Positions of long-term samples (LTS) in the ITER-like inner wall of JET during the discharge campaign 2013–2014. The numbers at the bottom indicate the octant number, where each octant is a 45° large sector of the torus. Tiles are numbered from top to bottom.

Table 1
A breakdown of neutral gas injection for the ILW-1 and ILW-2 discharge campaigns, measured in injected electrons.

	ILW-1	ILW-2
N2	6.889E + 24	2.642E + 25
Ne	2.208E + 22	1.254E + 24
H2	2.726E + 24	3.035E + 25
D2	2.518E + 26	3.721E + 26
3He	0	9.867E + 22
4He	0	5.236E + 21
Ar	5.249E + 22	1.543E + 23
Total	2.615E + 26	4.304E + 26

the recent 2013–2014 (ILW-2) campaign where somewhat higher power discharges with a total input energy of 200.5 GJ and an average input power of 2.82 MW, i.e. 20% higher than in ILW-1, were performed with a wider variation of discharge shapes and inner and outer strike points more often on the horizontal target tiles (Tiles 4 and 6). The ILW-2 campaign also had a significantly higher amount of neutral gas input (Table 1).

In this paper, experimental results from long-term samples (LTS) installed during the ILW-2 campaign at the RAIW between IWGLs are presented and compared to the results obtained with LTS during the ILW-1 campaign and the 2005–2009 JET-C campaign. A detailed comparison between the ILW-1 campaign and 2001–2004, 2005–2009 JET-C campaigns can be found in [11].

2. Experimental

Nine long-term samples (LTS) were exposed during the ILW-2 campaign and were identical to samples exposed in the ILW-1 campaign [11]. The samples were made from Inconel and mounted as inserts in beryllium coated Inconel tiles between IWGLs. The LTS surfaces were artificially roughened by sand-blasting, see [11] (Fig 1) for a scanning electron microscopy image. One half of the LTS surface was coated with tungsten using physical vapor deposition, the initial thickness of the tungsten layer was about 42 nm. The other half was coated with a Be layer of approximately 2.5 μm thickness.

Sample positions were identical to those during the ILW-1 campaign: Four samples were mounted in octant 4 at different poloidal locations (rows 2, 5, 8 and 11 counting from the top of the wall), five samples were mounted close to the inner midplane in the 8th row in different octants (octants 1, 2, 5, 6 and 8), see Fig. 1 [11]. The configuration of the inner wall was similar in both campaigns [20] with a surface area of 7.2 m^2 for the Be-coated RAIW and 4.0 m^2 for the W-coated RAIW. The areas were calculated based on the sizes of W-coated CFC at the top region of the RAIW section between two limiters (33,124 mm^2) and of the Be coated Inconel making up the rest of the RAIW region between two limiters (667,680 mm^2), and the distribution of W-coated CFC and Be coated Inconel surfaces on RAIW ([11] (Fig 1)).

The samples were analyzed using ion beam analysis methods before and after exposure. Elastic backscattering (EBS) using 1.6 MeV protons at a scattering angle of 165^0 was used to measure the layer thicknesses. The SIMNRA code [21] with SRIM 2013 [22] stopping powers was used for quantitative evaluation of the RBS spectra. See [11] for details of the analysis. To improve the accuracy in determining Be erosion the $^9Be(p,p)^9Be$ backscattering as well as the $^9Be(p,d)^8Be$ and $^9Be(p,\alpha)^6Li$ reactions cross-sections have been measured for the detector geometry with 165° scattering angle [23] and applied to the quantitative analysis of the measured spectra.

Net erosion rates were calculated from the amounts of the eroded material for all samples using the total time of successful ($I_p > 0.7$ MA) discharges obtained from JET discharge statistics (Table 2). For the condition where $I_p > 0.7$ MA is satisfied, the total plasma time of the ILW-2 campaign was about 10% longer than the plasma time of the ILW-1 campaign. Similarly, the durations of the limiter- and divertor-phases were about 10% longer in the ILW-2 campaign. It should be noted that because different publications [18] use slightly different discharge success thresholds, some discrepancies might exist in the erosion rate data.

3. Results and discussion

The poloidal and toroidal distributions of the erosion rates of Be and W during the ILW-2 campaign, as well as during the ILW-1, 2005–2009 (Be and C erosion) and 2001–2004 (W erosion) JET-C campaigns are shown in Fig. 2. Average RAIW erosion rates were

Table 2
JET discharge statistics for the ILW-1 and ILW-2 discharge campaigns.

Discharge campaign	Number of discharges	Total discharge time ($I_p > 0.7$ MA), 10^4 s	Divertor phase discharge time, 10^4 s	Limiter phase discharge time, 10^4 s	Total input energy, GJ
2011–2012	3812	6.41	4.51	1.90	150.6
2013–2014	4150	7.12	5.09	2.03	200.5

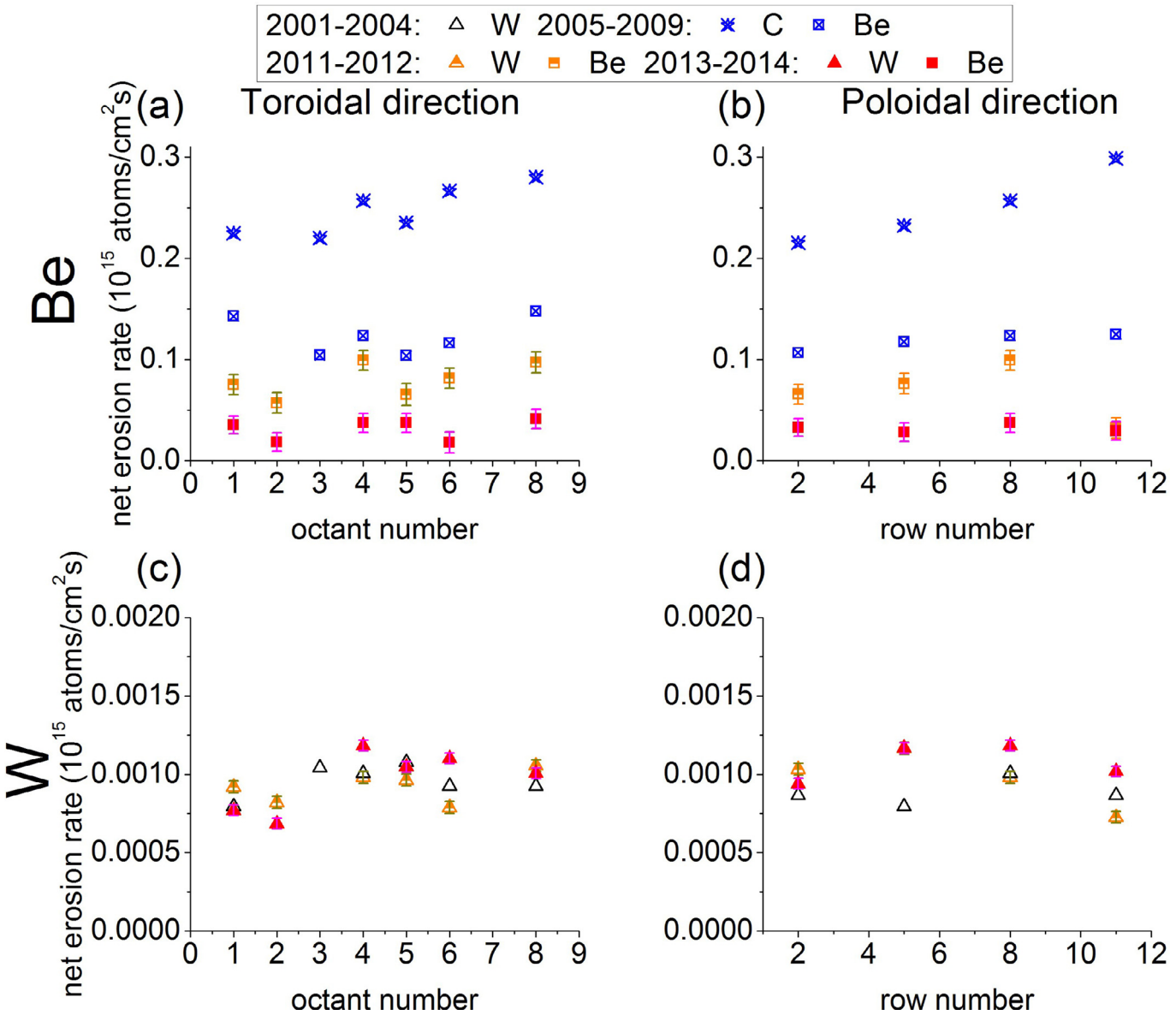

Fig. 2. Poloidal and toroidal distributions of the erosion rates of W and Be during the ILW-2 discharge campaign in comparison to the data for the ILW-1, 2005–2009 and 2001–2004 JET-C campaigns.

Table 3
Overview of LTS materials, average net total LTS erosion, and net erosion rates for the 2005–2009 JET-C, ILW-1 and ILW-2 campaigns.

Campaign	Sample material	Average total erosion, 10^{15} atoms/cm^2	Average erosion rate, atoms/cm^2·s
2005–2009	Be	36,000	$1.2 \cdot 10^{14}$
	C	74,000	$2.4 \cdot 10^{14}$
2011–2012	W	60	$9.2 \cdot 10^{11}$
	Be	3500	$5.5 \cdot 10^{13}$
2013–2014	W	63	$8.8 \cdot 10^{11}$
	Be	1900	$2.7 \cdot 10^{13}$

calculated based on the erosion data from the individual samples and are summarized in Table 2. In the following discussion W and Be RAIW erosion rates from ILW-2 are compared with ILW-1, all erosion rates are summarized in Table 3. A detailed comparison of the ILW-1 erosion with that from previous JET-C campaigns can be found in [11].

The net W erosion distribution was almost homogeneous in poloidal and toroidal directions for both the ILW-1 and ILW-2 campaigns (Fig 2c and d). The relative standard deviation (RSD), that is the standard deviation divided by the mean value, for the toroidal distribution was 0.11 and 0.2 for ILW-1 and ILW-2 respectively; 0.19 and 0.11 for the poloidal distributions in ILW-1 and ILW-2 respectively. The net erosion rates for the area near the mid-plane were almost the same for both campaigns (Fig 2c), differing by only about 5%. The average net erosion rates for the RAIW taking toroidal and poloidal variations into account are shown in Table 3 and are also almost the same. The total amount of W eroded from the W-coated areas of the RAIW during the whole

ILW-1 campaign was 0.7 g and 0.8 g for ILW-2 campaign based on the total erosion data (Table 3) in units of atoms/cm^2 multiplied by the surface area of the RAIW and by the atomic mass of W. For a hypothetical 11.2 m^2 full W RAIW, the total net erosion would have been about 2 g for ILW-1 campaign and 2.2 g for ILW-2. In terms of thickness, an average thickness of 9.3 nm W layer was removed during the ILW-1 campaign, and 10.2 nm in the ILW-2 campaign.

The toroidal distribution of the Be erosion remained the same in the ILW-2 campaign as in the ILW-1 campaign and was fairly homogenous (Fig 2a) (RSD of 0.22 and 0.33 for ILW1 and ILW-2, respectively). The poloidal distribution of Be erosion was also fairly homogenous (RSD = 0.13) and was similar to the erosion of Be samples measured during the 2005–2009 campaigns (Fig 2b). The net erosion rates for the area near the midplane differed by a factor of about two as shown in Fig. 2a: $7.9{\cdot}10^{13}$ atoms/cm^2 s for the ILW-1 campaign and $3.12{\cdot}10^{13}$ atoms/cm^2 s for the 2013–2014 campaign. The average net erosion rate for the RAIW taking toroidal and poloidal variations into account was also two times higher in the ILW-1 campaign than in the ILW-2 campaign (Table 3). The total amount of Be eroded from the Be-coated areas of the RAIW during the whole ILW-1 campaign was 3.8 g and 2.1 g for the ILW-2 campaign with a 5.5 g and 3.2 g erosion for a hypothetical full Be wall for the ILW-1 and ILW-2 campaigns, respectively. This translates to an average thickness of eroded Be of about 272 nm for ILW-1 and of about 158 nm for ILW-2.

While the W net erosion rate remained virtually the same, the Be erosion rate decreased by a factor of about two from the ILW-1 to the ILW-2 campaign. Erosion at these recessed areas is predominantly by charge-exchange neutral particles. Due to the high sputtering threshold energy of tungsten the erosion of tungsten is mainly caused by high-energetic particles originating from deeper inside the plasma. Beryllium is predominantly eroded by lower-energetic neutral particles originating from the edge plasma. The observed unchanged erosion rate of tungsten but decreased erosion rate of beryllium in higher power plasma discharges appears paradoxical at first sight. However, it could be explained by a decreased flux of lower-energetic neutral particles to the wall. This may be due to decreased neutral recycling fluxes, for example due to a larger mean clearance of the plasma to the inner wall, or due to a decreased plasma edge ion temperature. At the same time, the fluxes of high energetic particles from deeper inside the plasma seem not to have increased significantly by the only 20% increase in the average discharge power, resulting in an unchanged W erosion rate.

But it should be also kept in mind that net erosion measured by the method used in this paper is the difference between gross erosion and redeposition. A decrease of net erosion may be also the result of increased redeposition of material transported from other regions, caused for example by a higher beryllium erosion rate at the limiters.

Overall, the profound changes of main chamber wall erosion as observed during the ILW-1 campaign are confirmed by the observed inner-wall erosion during the ILW-2 campaign, where even lower net erosion rates are observed. Compared to the carbon net erosion rate during the 2005–2009 campaign the Be net erosion rate during the ILW-2 campaign decreased even further and was 9 times lower than the carbon erosion rate. The overall ratio of C Be and W erosion rates was C:Be:W≈270:31÷140:1, which shows higher relative erosion rates of Be and especially C than predicted in literature for ITER [24], likely due to the influence of low energy particles.

Further analysis of the erosion/deposition pattern on main chamber wall limiters and of the deposition pattern on divertor tiles in ILW-2 is still pending. Nevertheless, it can be already concluded that the profound change of the erosion/deposition pattern in JET was not an outlier of the ILW-1 campaign (caused for example by the limited applied heating power or the limited variation of plasma shapes), but is observed also in the ILW-2 campaign with somewhat increased heating power and different plasma shapes.

4. Conclusions

The erosion of Be and W marker layers was investigated using long-term samples (LTS) exposed during the ILW-2 campaign and was compared with the Be and W erosion data from the ILW-1 campaign and with C erosion from the 2005–2009 JET-C campaign. The marker layers were analyzed using elastic backscattering before and after exposure.

The W net erosion rate remained the same in all observed campaigns, both with respect to distribution and erosion rate. The toroidal distribution of the Be net erosion rate remained the same in the ILW-1 and ILW-2 campaigns. The poloidal distribution became more homogenous in ILW-2. The net erosion rate of Be decreased by a factor of about two from the ILW-1 to the ILW-2 campaign and was lower by a factor of about 9 than C net erosion in the 2005–2009 JET-C campaign. The profound change of the erosion/deposition pattern as observed during the ILW-1 campaign is confirmed in the ILW-2 campaign with respect to inner wall erosion, but further analysis of the erosion/deposition pattern on main chamber wall limiters and of the deposition pattern on divertor tiles is still necessary.

Acknowledgement

The technical assistance with ion beam measurements by J. Dorner and M. Fußeder is gratefully acknowledged.

This work has been carried out within the framework of the EUROfusion Consortium and has received funding from the Euratom research and training programme 2014–2018 under grant agreement No 633053. The views and opinions expressed herein do not necessarily reflect those of the European Commission.

References

[1] J.P. Coad, N. Bekris, J.D. Elder, S.K. Erents, D.E. Hole, K.D. Lawson, et al., Erosion/deposition issues at JET, J. Nucl. Mater. 290–293 (2001) 224–230, doi:10.1016/S0022-3115(00)00479-7.

[2] J.P. Coad, P. Andrew, D.E. Hole, S. Lehto, J. Likonen, G.F. Matthews, et al., Erosion/deposition in JET during the period 1999–2001, J. Nucl. Mater. 313–316 (2003) 419–423, doi:10.1016/S0022-3115(02)01403-4.

[3] J.P. Coad, P. Andrew, S.K. Erents, D.E. Hole, J. Likonen, M. Mayer, et al., Erosion and deposition in the JET MkII-SRP divertor, J. Nucl. Mater. 363–365 (2007) 287–293, doi:10.1016/j.jnucmat.2007.01.074.

[4] S. Krat, Y. Gasparyan, A. Pisarev, M. Mayer, U. von Toussaint, P. Coad, et al., Hydrocarbon film deposition inside cavity samples in remote areas of the JET divertor during the 1999–2001 and 2005–2009 campaigns, J. Nucl. Mater. 463 (2015) 822–826, doi:10.1016/j.jnucmat.2014.10.055.

[5] J. Likonen, J.P. Coad, D.E. Hole, S. Koivuranta, T. Renvall, M. Rubel, et al., Post-mortem measurements of fuel retention at JET with MKII-SRP divertor, J. Nucl. Mater. 390–391 (2009) 631–634, doi:10.1016/j.jnucmat.2009.01.176.

[6] S. Koivuranta, J. Likonen, A. Hakola, J.P. Coad, A. Widdowson, D.E. Hole, et al., Post-mortem measurements of fuel retention at JET in 2007–2009 experimental campaign, J. Nucl. Mater. 438 (Suppl) (2013) S735–S737. http://dx.doi.org/10.1016/j.jnucmat.2013.01.156.

[7] G.F. Matthews, Plasma operation with an all metal first-wall: Comparison of an ITER-like wall with a carbon wall in JET, J. Nucl. Mater. 438 (2013) S2–S10, doi:10.1016/j.jnucmat.2013.01.282.

[8] G.F. Matthews, M. Beurskens, S. Brezinsek, M. Groth, E. Joffrin, A. Loving, et al., JET ITER-like wall—overview and experimental programme, Phys. Scr. T145 (2011) 14001, doi:10.1088/0031-8949/2011/T145/014001.

[9] A. Baron-Wiechec, A. Widdowson, E. Alves, C.F. Ayres, N.P. Barradas, S. Brezinsek, et al., Global erosion and deposition patterns in JET with the ITER-like wall, J. Nucl. Mater. 463 (2015) 157–161, doi:10.1016/j.jnucmat.2015.01.038.

[10] M. Mayer, S. Krat, W. Van Renterghem, A. Baron-Wiechec, S. Brezinsek, I. Bykov, et al., Erosion and deposition in the JET divertor during the first ILW campaign, Phys. Scr. T167 (2016) 14051, doi:10.1088/0031-8949/T167/1/014051.

[11] S. Krat, Y. Gasparyan, A. Pisarev, I. Bykov, M. Mayer, G. de Saint Aubin, et al., Erosion at the inner wall of JET during the discharge campaign 2011–2012 in comparison with previous campaigns, J. Nucl. Mater. 456 (2015) 106–110, doi:10.1016/j.jnucmat.2014.08.010.

[12] J. Beal, A. Widdowson, K. Heinola, A. Baron-Wiechec, K.J. Gibson, J.P. Coad, et al., Deposition in the inner and outer corners of the JET divertor with carbon wall and metallic ITER-like wall, Phys. Scr. T167 (2016) 14052, doi:10.1088/0031-8949/T167/1/014052.
[13] S. Brezinsek, T. Loarer, V. Philipps, H.G. Esser, S. Grünhagen, R. Smith, et al., Long-term fuel retention in JET ITER-like wall, Nucl. Fusion. 53 (2013) 83023, doi:10.1088/0031-8949/T167/1/014075.
[14] M. Mayer, R. Behrisch, P. Andrew, J.P. Coad, A.T. Peacock, Transport and Redeposition of Eroded Material in JET, Phys. Scr. T81 (1999) 13, doi:10.1238/Physica.Topical.081a00013.
[15] M. Mayer, R. Behrisch, P. Andrew, A.T. Peacock, Erosion at the vessel walls of JET, J. Nucl. Mater. 241–243 (1997) 469–475, doi:10.1016/S0022-3115(97)80083-9.
[16] M. Mayer, R. Behrisch, K. Plamann, P. Andrew, J. Coad, A. Peacock, Wall erosion and material transport to the Mark I carbon divertor of JET, J. Nucl. Mater. 266–269 (1999) 604–610, doi:10.1016/S0022-3115(98)00834-4.
[17] M. Mayer, S. Krat, J.P. Coad, A. Hakola, J. Likonen, S. Lindig, et al., Erosion at the inner wall of JET during the discharge campaigns 2001–2009, J. Nucl. Mater. 438 (2013) S780–S783, doi:10.1016/j.jnucmat.2013.01.167.
[18] S. Brezinsek, A. Widdowson, M. Mayer, V. Philipps, P. Baron-Wiechec, J.W. Coenen, et al., Beryllium migration in JET ITER-like wall plasmas, Nucl. Fusion. 55 (2015) 63021, doi:10.1088/0029-5515/55/6/063021.
[19] F. Romanelli, Overview of the JET results with the ITER-like wall, Nucl. Fusion. 53 (2013) 104002, doi:10.1088/0029-5515/53/10/104002.
[20] M. Rubel, J.P. Coad, A. Widdowson, G.F. Matthews, H.G. Esser, T. Hirai, et al., Overview of erosion–deposition diagnostic tools for the ITER-Like Wall in the JET tokamak, J. Nucl. Mater. 438 (2013) S1204–S1207, doi:10.1016/j.jnucmat.2013.01.266.
[21] M. Mayer, SIMNRA User's Guide, Max-Planck-Institut für Plasmaphysik, Germany, Garching, Germany, 1997.
[22] J.F. Ziegler, SRIM.org, (n.d.).
[23] S. Krat, M. Mayer, C. Porosnicu, The 9Be(p,p0)9Be, 9Be(p,d0)8Be, and 9Be(p,α0)6Li cross-sections for analytical purposes, Nucl. Instruments Methods Phys. Res. Sect. B Beam Interact. with Mater. Atoms. 358 (2015) 72–81, doi:10.1016/j.nimb.2015.05.004.
[24] R. Behrisch, G. Federici, A. Kukushkin, D. Reiter, Material erosion at the vessel walls of future fusion devices, J. Nucl. Mater. 313–316 (2003) 388–392, doi:10.1016/S0022-3115(02)01580-5.